

GUARDIAN: Safety Filtering for Systems with Perception Models Subject to Adversarial Attacks

Nicholas Rober, Alex Rose, and Jonathan P. How

Abstract—Safety filtering is an effective method for enforcing constraints in safety-critical systems, but existing methods typically assume perfect state information. This limitation is especially problematic for systems that rely on neural network (NN)-based state estimators, which can be highly sensitive to noise and adversarial input perturbations. We address these problems by introducing GUARDIAN: Guaranteed Uncertainty-Aware Reachability Defense against Adversarial INterference, a safety filtering framework that provides formal safety guarantees for systems with NN-based state estimators. At runtime, GUARDIAN uses neural network verification tools to provide guaranteed bounds on the system’s state estimate given possible perturbations to its observation. It then uses a modified Hamilton-Jacobi reachability formulation to construct a safety filter that adjusts the nominal control input based on the verified state bounds and safety constraints. The result is an uncertainty-aware filter that ensures safety despite the system’s reliance on an NN estimator with noisy, possibly adversarial, input observations. Theoretical analysis and numerical experiments demonstrate that GUARDIAN effectively defends systems against adversarial attacks that would otherwise lead to a violation of safety constraints.

I. INTRODUCTION

Neural network (NN)-based machine learning continues to demonstrate its utility as a tool for building autonomous systems with impressive capabilities [1]. However, NNs are sensitive to input perturbations [2], posing a significant safety risk associated with their application [3]. This threat is exacerbated for systems with NN-based perception modules, i.e., observation-based neural feedback loops (ONFLs), because adversarial agents can manipulate system-level behavior by attacking the perception model’s observations [4]. Thus, it is important to develop protective methods for systems with learned perception modules subject to adversarial attacks before they can be applied in safety-critical scenarios.

In response to the threat posed by adversarial attacks, NN verification (NNV) has become an active area of research. A wide range of open-loop verification techniques [5]–[7] have been developed to calculate guaranteed bounds on an NN output given a nominal input and a set of possible perturbations. These ideas have been extended to design-time verification of closed-loop systems, primarily via set-propagation-based reachability analysis techniques, for systems with NN controllers [8], [9] and, less frequently, ONFLs [10], [11]. While [10], [11] shows how NNV can be used

Submitted February 4th, 2026. This material is based upon work supported by the Naval Information Warfare Center (NIWC) Atlantic under Contract No. N6523623C8011. The views, opinions, and/or findings expressed are those of the author(s) and should not be interpreted as representing the official views or policies of the Department of Defense or the U.S. Government.

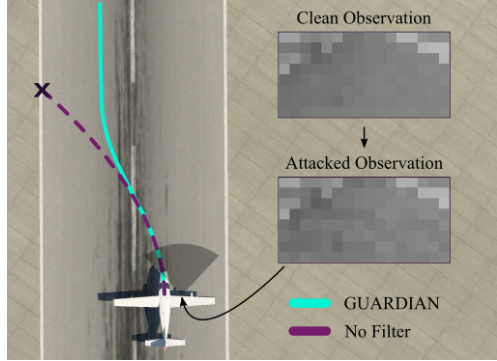


Fig. 1: GUARDIAN protects against adversarial attacks.

for ONFLs prior to deployment, it is difficult to incorporate a priori unknown perturbations from adversarial attacks that are infused at runtime. Recently, [11] accomplished this by employing Hamilton-Jacobi (HJ) reachability analysis, but their approach is dependent on an abstraction of the closed-loop system that is difficult to obtain for complicated control pipelines. Thus, to protect ONFLs from adversarial attacks, we instead consider runtime safety assurances.

Safety filtering [12], [13], i.e., modifying nominal control inputs to ensure satisfaction of safety constraints, is a common approach to ensure safety at runtime. Recent work has shown that NNV tools can be used as a runtime safety monitor [14], but they have not yet been demonstrated as a means of safety filtering. Instead, most safety filters are constructed using either control barrier functions (CBFs) [15] or Hamilton-Jacobi reachability analysis [16]. While most work on safety filtering assumes perfect state information, several recent works have focused on incorporating observation models and accounting for imperfect state information [17]–[20]. Namely, [17] proposed a measurement-robust (MR)-CBF formulation that accounts for state-dependent measurement error via a more restrictive CBF condition. Furthermore, [18] developed an alternative robust (R)-CBF method that similarly accounts for measurement error and is guaranteed to exist if there exists a normal CBF, but does not capture state-dependent estimation error. Additionally, R-CBFs are proven to be invariant for an inflated region around the original safe set, leading to conservative behavior or possible safety violations. Finally, [19] extends [18] by adaptively tuning an R-CBF to be less conservative and capture state-dependent error, but again is invariant for an inflated version of the safe set. Moreover, while [17]–[19] all incorporate measurement error, determining that error in the context of adversarial attacks has not yet been explored.

In contrast to [17]–[19], this paper proposes an HJ-reachability-based safety filter, GUARDIAN: Guaranteed Uncertainty-Aware Reachability Defense against Adversarial INterference. GUARDIAN uses state-of-the-art NNV tools to compute state uncertainty given a nominal observation and a bound on the strength of possible adversarial attacks. This uncertainty set is then incorporated into a modified HJ-reachability formulation that filters potentially unsafe nominal control inputs, ensuring provably safe closed-loop behavior under adversarial influence. We present several examples illustrating key features of GUARDIAN, including its ability to protect image-based ONFLs, its handling of state-dependent vulnerability to adversarial attacks, and its performance relative to MR-CBFs [17], R-CBFs [18], and R-CBF-QPs [19]. The main contributions of this work include:

- A modified HJ reachability formulation that incorporates state-estimation uncertainty, enabling safety guarantees for single-input systems with estimation modules subject to noisy or adversarially perturbed observations.
- GUARDIAN: a unified safety-filtering framework that combines our modified HJ reachability with modern NNV techniques to protect systems with NN-based perception modules from adversarial attacks.
- Numerical examples demonstrating GUARDIAN’s effectiveness in safeguarding ONFLs against adversarial manipulation and comparing its performance to CBF-based approaches [17]–[19].

II. PRELIMINARIES

A. System Dynamics

Consider the nonlinear discrete time system with state vector $x_k \in \mathcal{X} \subseteq \mathbb{R}^{n_x}$ and control-affine dynamics

$$x_{t+1} = f_d(x_t, d_t) + g(x_t)u_t \triangleq f(x_t, u_t, d_t) \quad (1)$$

where $u_t \in [\underline{u}, \bar{u}] \triangleq \mathcal{U} \subset \mathbb{R}$ is the scalar control input, and $d_t \in \mathcal{D}^x \subset \mathbb{R}^{n_x}$ is the disturbance term capturing the predictive uncertainty of the system due to unknown external forces, actuator degradation, and modeling error. While our approach may work in practice for multidimensional u , we consider the scalar case here due to improved interpretability of the theoretical argument presented in §III-A. The system has a sensor providing measurements $y_t \in \mathcal{Y} \subseteq \mathbb{R}^{n_y}$ from the environment according to the function $y_t = h(x_t, d_t^y)$ where $d_t^y \in \mathcal{D}^y$ represents possible sensor noise. The sensor measurements are passed to an NN estimator $L_\theta : \mathcal{Y} \rightarrow \mathcal{X}$, which provides estimates of the system’s state \hat{x}_t , i.e., $\hat{x}_t = L_\theta(y_t)$. The system also has a controller $K_d : \mathcal{X} \rightarrow \mathcal{U}$, which generates an input u_t based on the state estimate from L_θ . Finally, the system is subject to safety constraints, which can be encoded by designing a function $c : \mathcal{X} \rightarrow \mathbb{R}$ such that $\mathcal{C} \triangleq \{x \mid c(x) \leq 0\}$, (e.g., a signed distance function), represents the set of unsafe states.

B. Adversarial Attacks

Adversarial attacks are constructed perturbations to an NN’s input that cause it to behave in an undesirable way. In this work, we implement a targeted attack using the projected

gradient descent (PGD) method outlined below: Given a nominal input $y \in \mathbb{R}^{n_y}$, a target output $x^* \in \mathbb{R}^{n_x}$, and a maximum perturbation $\epsilon \in \mathbb{R}_{>0}$, we iteratively construct an adversarial attack $\Delta y \in \mathbb{R}^{n_y}$ against an NN $\pi : \mathcal{Y} \rightarrow \mathcal{X}$ via

$$\begin{aligned} \Delta y^{(k+1)} &= P_{\mathcal{B}_\epsilon} \left(\Delta y^{(k)} - \alpha \text{sgn}(\nabla_{\tilde{y}^{(k)}} J(\pi(\tilde{y}^{(k)}), x^*)) \right) \quad (2) \\ \Delta y^{(0)} &= 0^{n_y}, \quad k = 0, \dots, n_{pgd} - 1 \end{aligned}$$

where $\alpha \in \mathbb{R}_{>0}$ is the step size parameter, $n_{pgd} \in \mathbb{Z}_{>0}$ is the number of iterations, $\tilde{y}^{(k)} \triangleq y + \Delta y^{(k)}$, $\Delta y \triangleq \Delta y^{(n_{pgd})}$, $P_{\mathcal{B}_\epsilon}(\cdot)$ is a projection operator that maps its input into the ℓ_∞ ball with radius ϵ centered at 0, $\text{sgn}(\cdot)$ returns the element-wise sign of an input, and $J : \mathcal{X} \times \mathcal{X} \rightarrow \mathbb{R}$ is a cost function, e.g., mean-squared error. The result from (2) is an attack Δy that satisfies the condition $\|\Delta y\|_\infty \leq \epsilon$ and approximately minimizes the distance between the target x^* and the adversarially perturbed NN output $\hat{x} = \pi(\tilde{y})$, where $\tilde{y} \triangleq y + \Delta y$. As will be shown later, this strategy can be used to trick a system with an NN-based estimator to violate safety if it is not equipped with a safety filter designed to protect against adversarial attacks.

C. Neural Network Verification

Neural network verification (NNV) refers to a set of techniques that formally analyze the computation patterns of a given NN to make statements about its behavior as follows:

Theorem 1 (NN Robustness Verification [5]): Given a neural network $\pi : \mathbb{R}^{n_z} \rightarrow \mathbb{R}^{n_o}$ and a hyper-rectangular set of possible inputs \mathcal{Z} , there exist two explicit functions

$$\underline{\pi}(z) = \Psi z + \alpha, \quad \bar{\pi}(z) = \Xi z + \beta \quad (3)$$

such that the inequality $\underline{\pi}(z) \leq \pi(z) \leq \bar{\pi}(z)$ holds element-wise for all $z \in \mathcal{Z}$, with $\Psi, \Xi \in \mathbb{R}^{n_o \times n_z}$ and $\alpha, \beta \in \mathbb{R}^{n_o}$. Theorem 1 is proven in [5] and implemented so that the bounds $\underline{\pi}(z)$ and $\bar{\pi}(z)$ can be found using tools such as CROWN [5], auto_LiRPA [6], and jax_verify [7].

D. Hamilton-Jacobi Reachability Analysis

Hamilton-Jacobi (HJ) reachability analysis is an optimal control approach that poses reachability as a two-player game with worst-case disturbances pushing the system out of the safe set and control inputs acting in opposition, attempting to keep the system safe. In discrete-time HJ reachability analysis, the solution to the Isaacs equation [21] can be obtained from dynamic programming via

$$\begin{aligned} V_k(x) &= \min \left(c(x), \max_{u \in \mathcal{U}} \min_{d \in \mathcal{D}^x} V_{k+1}(f(x, u, d)) \right) \quad (4) \\ k &\in \{0, 1, \dots, T-1\}, \quad V_T(x) = c(x). \end{aligned}$$

The value function $V(x) = \lim_{k \rightarrow \infty} V_k(x)$ encodes the set of states for which there exists some action that the system can take to guarantee safety from disturbances. Conversely, if $V(x) < 0$, there is some sequence of disturbances that can cause a safety violation, i.e., $c(x_T) \leq 0$, for any sequence of control inputs. Using $V(x)$, we can construct the maximal

safe set $\Omega^* \triangleq \{x \in \mathcal{X} \mid V(x) \geq 0\}$ with a boundary $\partial\Omega^* \triangleq \{x \in \mathcal{X} \mid V(x) = 0\}$ and safe control policy $u_{HJ}^*(x)$:

$$u_{HJ}^*(x) \in \arg \max_{u \in \mathcal{U}} \min_{d \in \mathcal{D}} V(f(x, u, d)). \quad (5)$$

An HJ-based safety filter can then be constructed using the switching function

$$K_{F,\text{nom}}(x, u) \triangleq \begin{cases} u, & \min_{d \in \mathcal{D}} V(f(x, u, d)) \geq 0 \\ u_{HJ}^*, & \text{otherwise,} \end{cases} \quad (6)$$

which ensures that if the unfiltered input u causes the system to leave Ω^* , then the safety filter will be activated.

III. GUARDIAN

As introduced in §I, GUARDIAN is a safety filtering approach that incorporates measurement uncertainty determined via NNV into a modified HJ reachability formulation to design a safe control policy. The first key idea in GUARDIAN is to use NNV to determine a set containing all possible states $\bar{\mathcal{X}}_t$ given an adversarially perturbed \tilde{y}_t . Given that the perturbation $\|\Delta y\|_\infty \leq \epsilon$, we know the true observation is contained by the set $\bar{\mathcal{Y}}_t \triangleq \{y_t \mid \|y_t - \tilde{y}_t\|_\infty \leq \epsilon\}$. Applying Theorem 1, we can then use NNV tools to generate upper and lower bounds on the output of L_θ , i.e., \tilde{x}_t and \tilde{x}_t , respectively, such that the adversarially perturbed state estimate $\hat{x}_t \in [\tilde{x}_t, \bar{x}_t]$. Given bounds $e_{\hat{x}} \in \mathbb{R}_{\geq 0}^{n_x}$ on the state estimation error without adversarial perturbations, i.e., $|\hat{x}_{t,i} - x_{t,i}| \leq e_{\hat{x},i} \forall i \in \{1 \dots n_x\}$, we then construct

$$\bar{\mathcal{X}}_t \triangleq [\tilde{x}_t - e_{\hat{x}}, \bar{x}_t + e_{\hat{x}}], \quad (7)$$

where it can then be shown that $x_t \in \bar{\mathcal{X}}_t$. Defining $\Phi(\bar{\mathcal{X}}_t, u) \triangleq \min_{s \in \bar{\mathcal{X}}_t, d \in \mathcal{D}^x} V(f(s, u_t, d))$, reformulate (6):

$$K_F(\bar{\mathcal{X}}_t, u_t) \triangleq \begin{cases} u_t, & \Phi(\bar{\mathcal{X}}_t, u_t) \geq 0 \\ u_{HJ}^*, & \text{otherwise,} \end{cases} \quad (8)$$

where the optimal safe control policy now becomes

$$u_t^*(\bar{\mathcal{X}}_t) \in \arg \max_{u \in \mathcal{U}} \Phi(\bar{\mathcal{X}}_t, u). \quad (9)$$

A. Theoretical Results

To validate the safety of GUARDIAN, we then introduce Assumptions 1 and 2, along with Lemma 1 and Theorem 2. Assumptions 1 and 2 provide sufficient conditions to ensure there is a uniform safe control direction for any $s \in \bar{\mathcal{X}}_t$ and provide that $\bar{\mathcal{X}}_t$ is a reasonable size relative to Ω^* .

Assumption 1: There exists a neighborhood $\mathcal{N}(\partial\Omega^*) \supset \partial\Omega^*$ such that $V \in C^1(\mathcal{N}(\partial\Omega^*))$ and for any convex $\mathcal{S} \subset \mathcal{N}(\partial\Omega^*)$, there is a safe control cone $\mathcal{K}(\mathcal{S})$ where

$$\nabla V(s)^\top g(s) u \geq 0 \quad \forall s \in \mathcal{S}, \forall u \in \mathcal{U} \cup \mathcal{K}(\mathcal{S}). \quad (10)$$

Assumption 2: The attack strength ϵ and error term $e_{\hat{x}}$ are sufficiently small to give $\bar{\mathcal{X}}_t \subset \mathcal{N}(\partial\Omega^*)$ and $f(s, u, d) \in \mathcal{N}(\partial\Omega^*) \forall s \in \bar{\mathcal{X}}_t, \forall u \in \mathcal{U}, \forall d \in \mathcal{D}^x$ if $\Phi(\bar{\mathcal{X}}_t, u_t) < 0$.

Note that Assumption 1 can be checked offline while Assumption 2 must be checked at runtime due to the complicated relationship between L_θ and possible input perturbations. As shown in §IV, these assumptions allow

the application of GUARDIAN in a variety of practical situations. Moreover, they are not strictly necessary, e.g., $\bar{\mathcal{X}}_t$ may leave $\mathcal{N}(\partial\Omega^*)$ and the system will remain safe so long as $\bar{\mathcal{X}}_t \setminus \mathcal{N}(\partial\Omega^*) \subset \Omega^*$.

Lemma 1: Let Assumptions 1 and 2 hold for $\mathcal{S} \subset \mathcal{N}(\partial\Omega^*)$ and $u_1, u_2 \in \mathcal{U}$ satisfy $u_2 - u_1 \in \mathcal{K}(\mathcal{S})$. Then $V(f(s, u_1, d)) \leq V(f(s, u_2, d)) \forall s \in \mathcal{S}, \forall d \in \mathcal{D}^x$.

The proof for Lemma 1 follows directly from integrating the monotonicity condition (10) from u_1 to u_2 .

Theorem 2: Consider a system with dynamics (1), safe set Ω^* , and true initial state $x_0 \in \Omega^*$. If Assumptions 1 and 2 hold, then for each $t \in \mathbb{Z}_{\geq 0}$, constructing $\bar{\mathcal{X}}_t$ as specified in (7) and applying the safety filter (8) results in $x_t \in \Omega^*$, thereby rendering Ω^* an invariant set.

Proof: We proceed by induction, showing that $x_t \in \Omega^* \implies x_{t+1} \in \Omega^*$, where the base case $x_0 \in \Omega^*$ holds by assumption. Then, for the inductive step, suppose $x_t \in \Omega^*$ and recognize that the filter is either (i) inactive (first case in (8)), or (ii) active (second case (8)). For the inactive case, the nominal control value u_t results in $\Phi(\bar{\mathcal{X}}_t, u_t) \geq 0$, so $\forall s \in \bar{\mathcal{X}}_t, \forall d \in \mathcal{D}^x, V(f(s, u_t, d)) \geq 0$. Since $V(s) \geq 0 \iff s \in \Omega^*$, $x_{t+1} \in \Omega^*$ follows for the inactive case.

For the active case, $\Phi(\bar{\mathcal{X}}_t, u_t) < 0$, so by Assumption 2 we have $\bar{\mathcal{X}}_t \subset \mathcal{N}(\partial\Omega^*)$. If calculating u^* via (9) results in $\Phi(\bar{\mathcal{X}}_t, u^*) \geq 0$, then, similar to the inactive case, we get $x_{t+1} \in \Omega^*$ directly. Alternatively, if $\Phi(\bar{\mathcal{X}}_t, u^*) < 0$, recall that $x_t \in \Omega^*$, where, by construction of Ω^* , $\exists u^\dagger(x_t) \in \mathcal{U}$ such that $\min_{d \in \mathcal{D}^x} V(f(x_t, u^\dagger(x_t), d)) \geq 0$ [21]. From Assumptions 1 and 2, there is a safe control cone $\mathcal{K}(\bar{\mathcal{X}}_t)$ where $\mathcal{K}(\bar{\mathcal{X}}_t) \in \{\mathbb{R}_{\leq 0}, \mathbb{R}_{\geq 0}, \mathbb{R}\}$ for scalar u . If $\mathcal{K}(\bar{\mathcal{X}}_t) = \mathbb{R}_{\geq 0}$ and $\Phi(\bar{\mathcal{X}}_t, u^*) < 0$, then the monotonicity condition (10) and Lemma 1 can be used to show that $u^* = \bar{u}$, so $u^* \geq u^\dagger(x_t)$ and $u^* - u^\dagger(x_t) \in \mathcal{K}(\bar{\mathcal{X}}_t)$. A similar argument can be made for $\mathcal{K}(\bar{\mathcal{X}}_t) = \mathbb{R}_{\leq 0}$. Lemma 1 then results in

$$V(f(s, u^\dagger(x_t), d)) \leq V(f(s, u^*, d)) \quad \forall s \in \bar{\mathcal{X}}_t, \forall d \in \mathcal{D}^x. \quad (11)$$

Finally, if $\mathcal{K}(\bar{\mathcal{X}}_t) = \mathbb{R}$, then $\nabla V(s)^\top g(s) = 0 \forall s \in \bar{\mathcal{X}}_t$, so

$$V(f(s, u^\dagger(x_t), d)) = V(f(s, u^*, d)) \quad \forall s \in \bar{\mathcal{X}}_t, \forall d \in \mathcal{D}^x. \quad (12)$$

Considering Eqs. (11) and (12) for x_t specifically, we get $V(f(x_t, u^\dagger(x_t), d)) \leq V(f(x_t, u^*, d)) \forall d \in \mathcal{D}^x$ for each possible instance of $\mathcal{K}(\bar{\mathcal{X}}_t)$, so $\min_{d \in \mathcal{D}^x} V(f(x_t, u^*, d)) \geq 0$ and $x_{t+1} \in \Omega^*$ for the active case, completing the proof. ■ Intuitively, this proof shows that at each time step, if the filter is active, GUARDIAN pushes the true state in a safe direction, resulting in safety at the next time step. Interestingly, this does not mean that $\min_{s \in \bar{\mathcal{X}}_t} V(s) \geq 0$ at every time step. In fact, as shown in §IV, it may be true that for some t , $\min_{s \in \bar{\mathcal{X}}_t} V(s) < 0$ (e.g., due to varying sensitivity to Δy), but the proof holds because in that case, the true state x_t is still pushed towards the interior of Ω^* .

B. Scalability

There are two scalability considerations associated with this approach. First, the scalability of the NNV component with respect to NN size depends on the specific NNV

tool used and can be expected to improve as verification methods advance. In this work, we use CROWN [5], which has polynomial time complexity in both the number of layers and neurons per layer in L_θ . Second, the scalability limitations of HJ reachability are well known [16], since solving (4) typically requires discretizing the state space, leading to exponential complexity in the state dimension. In future work, we plan to explore applying GUARDIAN with learned [22] and latent-space [23] reachability methods to improve scalability.

IV. NUMERICAL RESULTS

This section presents several examples demonstrating GUARDIAN and its properties, including comparisons to several CBF-based approaches. All experiments were conducted on a machine running Ubuntu 22.04 with an i7-6700K CPU and 32 GB of RAM using `jax-verify` [7] for NNV and the `hj_reachability` python toolbox [24].

A. Taxinet Safety

We first demonstrate GUARDIAN on a runway taxiing problem similar to [10]. Consider an aircraft with state $x = [p_x, p_y, \theta]^\top$, where p_y and θ represent the cross-track error (CTE) and the heading error (HE), measured from the centerline of the runway, respectively, and p_x is the down-track position (DTP). The dynamics of the aircraft are

$$\begin{aligned} p_{x,t+1} &= p_{x,t} + T_s (v \cos(\theta_t) + d_t^x) \\ p_{y,t+1} &= p_{y,t} + T_s (v \sin(\theta_t) + d_t^y) \\ \theta_{t+1} &= \theta_t + T_s \left(\frac{v}{\ell} \tan\left(\frac{\pi}{180} \phi_t\right) + d_t^\theta \right), \end{aligned}$$

where $v = 5.0$ m/s is the constant velocity of the aircraft, $\ell = 5.0$ m is the distance between its front and back wheels, $\phi_t \in [-12^\circ, 12^\circ]$ is the rudder angle, $T_s = 0.1$ s, $|d_t^x|, |d_t^y| \leq 0.02$ m, and $|d_t^\theta| \leq 0.01$ rad. Realistic images of a runway scenario are obtained by simulating the dynamics in X-Plane 11, providing 8×16 resolution downsampled images which are passed into the NN estimator L_θ discussed in [10]. There is a simple nominal controller (proportional control) given by $K_d(x_t) = -0.74p_{x,t} - 0.44\theta_t$. The safe set is defined by the runway boundary, i.e., $\mathcal{C}^c \triangleq \{x \mid |p_{x,t}| \leq 10\}$.

As presented in [10], [11], under nominal conditions, the estimator L_θ and controller K_d are guaranteed to keep the system safe under most initial conditions. However, Fig. 2 shows a trajectory (dashed purple) demonstrating that safety can be violated as a result of an adversarial attack ($\epsilon = 0.021$) on the aircraft if it does not have a filter. In contrast, when the system uses GUARDIAN from the same initial condition (solid black), it calculates $\bar{\mathcal{X}}_t$ (shaded teal) and uses the filter (8) to successfully stay on the runway while achieving a total per-step calculation time of 0.032 ± 0.003 s. Moreover, to validate Theorem 2, we generated 100,000 sample trajectory rollouts ξ_i (light teal), where $\xi_i = \{x'_t | x'_{t+1} = P_{\bar{\mathcal{X}}_t}(f(x'_t, u_t, d_t)), d_t \sim \mathcal{D}^x \forall t \in [0, T]\}_i$ with each $\{x_0\}_i \sim \mathcal{X}_0$ and where $P_{\bar{\mathcal{X}}_t}(\cdot)$ projects a state x'_t into $\bar{\mathcal{X}}_t$ to enforce that it is valid given the observation \tilde{y}_t ,

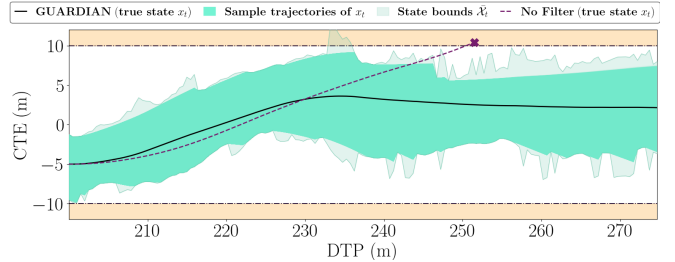


Fig. 2: Trajectories of a taxiing aircraft subject to adversarially perturbed observations with and without GUARDIAN.

i.e., $\exists d^y \in \mathcal{D}^y$ such that $L_\theta(h(x'_t, d^y)) \in \bar{\mathcal{Y}}_t$ as discussed in §III-A. As shown in Fig. 2, even though $\bar{\mathcal{X}}_t$ leaves the safe set between 233 and 236 m, each ξ_i remains safe. This connects to the proof of Theorem 2 because if $\Phi(\bar{\mathcal{X}}_t, u_t) < 0$, then $K_F(\bar{\mathcal{X}}_t, u_t) \rightarrow -12$, which is the maximal right-hand turn and any $x'_t \in \bar{\mathcal{X}}_t$ will move in a safe direction.

B. State-Dependent Vulnerability to Adversarial Attacks

This section shows how GUARDIAN uses NNV to account for and protect against the state-estimate's sensitivity to measurement perturbations. Consider the system with state vector $x = [p_x, p_y, v_x, v_y]^\top$ and dynamics

$$\begin{aligned} p_{t+1} &= p_t + T_s \left(v_t + \frac{1}{2} T_s u_t + d_t^p \right) \\ v_{t+1} &= v_t + T_s (u_t + d_t^v), \end{aligned} \quad (13)$$

where $p = [p_x, p_y]^\top$, $v = [v_x, v_y]^\top$, and $u = [u_x, u_y]^\top$ with $\|u_t\|_\infty \leq 5.0$, $T_s = 0.1$, $\|d_t^p\|_\infty \leq 1e^{-5}$, and $\|d_t^v\|_\infty \leq 1e^{-5}$. Range measurements are taken from a set of landmarks $\ell_i \in \mathbb{R}^2$, $i \in \{1, 2, 3, 4\}$ such that for each time step, $y_t \in \mathbb{R}^4$ has elements obtained via $y_{t,i} = \|\ell_i - p_t\| + \Delta y_t$, where Δy_t is obtained via (2) and satisfies $\|\Delta y_t\|_\infty \leq \epsilon$ with $\epsilon = 0.05$. We use a learned estimator L_θ trained to predict \hat{x} using a history of three measurements $y_{t:t-2}$, i.e., $\hat{x}_t = L_\theta(y_{t:t-2})$. The nominal controller $K_d(\hat{x}, t)$ is designed to track a circle-like trajectory (shown in Fig. 3) that is inset within a 10×10 m region defining the safe set. The attack Δy_t is designed to bring \hat{x}_t towards the center of the circle, resulting in the true state x_t trending radially outward toward the unsafe region. Note that (13) decomposes into $x - y$ components, each with a scalar input.

Each panel of Fig. 3 shows twenty sample trajectories using standard HJ safety filtering (6) (top row), and GUARDIAN (bottom row) for square (left column) and triangular (right column) landmark configurations. The trajectories are colored to show the amount of estimation error affecting the system at different points throughout each trajectory, indicating how effective the adversarial attack was in different regions. When compared with the square landmark configuration on the left, the right plots show that the triangular landmark configuration results in trajectories with more error, especially near the top left and bottom right portions of their rollouts. Interestingly, GUARDIAN detects this increase in error and acts more conservatively in those

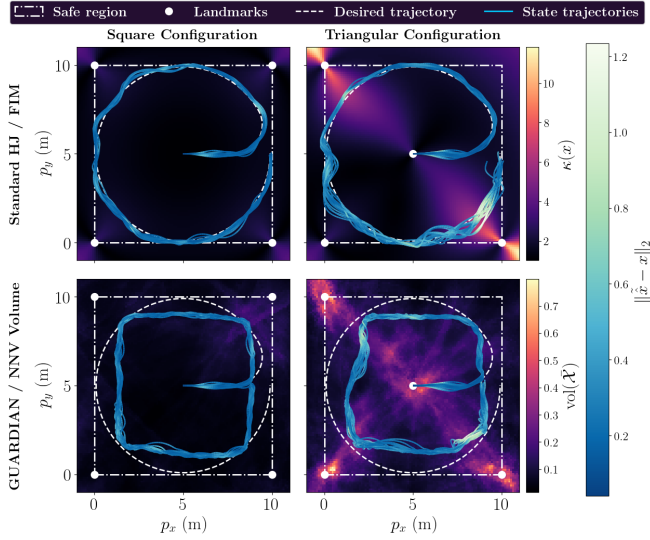


Fig. 3: State error for sample trajectories with different landmark configurations show state-dependent vulnerability to adversarial attacks. Triangular landmarks (right) are more vulnerable to attack than square landmarks (left). Standard HJ reachability (top) does not ensure safety, but GUARDIAN (bottom) does by quantifying state uncertainty. Heatmaps show trends from FIM condition number (top) are captured by NNV set volume (bottom).

regions, as shown by the deflection of the trajectories when compared with the square configuration.

The triangular configuration trajectories also show that the attack is more effective along the diagonal on which most of the landmarks are aligned, which makes intuitive sense because in those regions there is redundant information along the diagonal and less information orthogonal to it. To solidify this point, we consider an analog to the Fisher information matrix (FIM) [25]: $I(x) = \frac{1}{\epsilon^2} J^\top J$, where $J \triangleq \frac{\partial h}{\partial x}$. We can then quantify the quality of information received by a measurement at x via the condition number $\kappa(x) \triangleq \frac{\lambda_1(I(x))}{\lambda_2(I(x))}$, where $\lambda_1(I(x))$ and $\lambda_2(I(x))$ are the first and second largest eigenvalues of $I(x)$, indicating how sensitive a measurement at x is to perturbations. The heatmap in Fig. 3 (top) shows the FIM condition number $\kappa(x)$ for both configurations of landmarks. Larger condition numbers indicate measurements with worse information (i.e., those more sensitive to perturbations), so the heatmaps confirm the previously described intuition by showing that the state estimate error increases in poorly conditioned regions.

For comparison to $\kappa(x)$, the heatmaps in the bottom plots of Fig. 3 show the volume of the state bounds, i.e., $\text{vol}(\bar{\mathcal{X}})$, obtained using NNV with observations at each x subject to ϵ perturbations. As shown by comparing the two right plots, NNV captures similar trends in measurement sensitivity to those calculated analytically with the FIM. This capability enables GUARDIAN to incorporate state-dependent sensitivity analysis into its filtering approach, resulting in a filter that is appropriately conservative depending on varying levels of vulnerability to adversarial attacks. As a result, GUARDIAN (bottom) acts as an effective safety

filter, ensuring all trajectories stay within the 10×10 bounds, whereas the standard HJ formulation (top) does not.

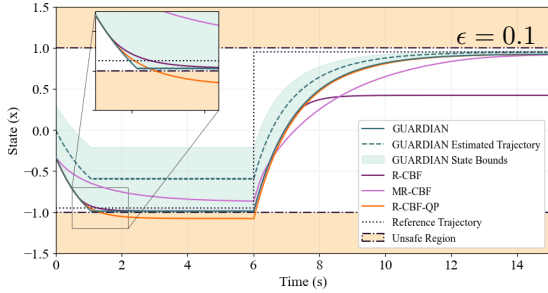
C. Comparison to MR-CBFs, R-CBFs, and R-CBF-QPs

Measurement-Robust CBFs (MR-CBFs) [17], Robust CBFs (R-CBFs) [18], and adaptive robust CBFs (R-CBF-QPs) [19] were not specifically designed for defense against adversarial attacks, but their handling of state uncertainty in safety-critical settings means they could be adapted for such purposes. Thus, to highlight key differences between these approaches and GUARDIAN, we consider the scalar system with dynamics $x_{t+1} = x_t + T_s(u_t + d_t^x)$ with $K_d(x, t) = x_{ref,t} - x_t$ and with a nonlinear observation function $y_t = \frac{1}{4} \log \left(\frac{4}{x_t+3} - 1 \right) + d_t^y$ where $|d_t^y| \leq \epsilon$. Solving for x_t in terms of y_t then gives $L(y_t) \triangleq 4 \cdot \text{sigmoid}(4y_t - d_t^y) - 3$, which acts as a perfect estimator in the absence of noise. The safe set for this system is the region bounded by $[-1, 1]$, i.e., $\mathcal{C}^c = \{x \mid |x| \leq 1\}$.

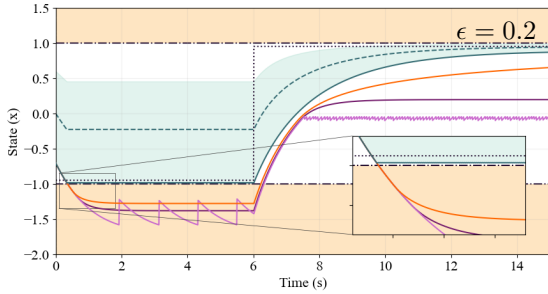
Fig. 4a shows that GUARDIAN is less conservative than both MR-CBFs and R-CBFs and satisfies the safety constraint where the R-CBF-QP does not. For each filter, the initial state estimate is $\hat{x}_0 = 0$ and the disturbance term d_t^y is set at a constant value of $\epsilon = 0.1$, resulting in the true state x_t always being at the lower bound of possible values given the measurement model and possible noise. The reference value is set to $x_{ref} = -0.95$ for $t \in [0, 6]$ and $x_{ref} = 0.95$ for $t \in [6, 15]$. Like the case in §IV-B, the shaded NNV state bounds $\bar{\mathcal{X}}_t$ about the state estimate \hat{x}_t for GUARDIAN (dashed teal) show that the measurements are much more sensitive to perturbations near the lower boundary than near the upper boundary. Using the resulting state bounds, GUARDIAN allows the state estimate to converge to x_{ref} when it is set near the upper boundary, but intervenes at the lower boundary to ensure x_t (solid teal) stays in the safe set.

By comparison, R-CBFs assume a maximum state error and thus do not account for state-dependent bounds. As a result, the R-CBF (purple) is appropriately conservative at the lower boundary where the state error is at its largest, but it is similarly conservative at the upper boundary, which is unnecessary given the better measurements in that region of the state space. The R-CBF-QP (orange) is an adaptively tuned version of the R-CBF, so it is less conservative. However, since it is invariant for an inflated version of \mathcal{C}^c , it violates safety at the lower boundary. Finally, the MR-CBF (pink) uses the same state bounds as GUARDIAN, but is more conservative in its transient and steady state behavior.

Moreover, as shown in Fig. 4b, each of the CBF-based approaches suffer from performance degradation in the presence of large estimation error. Above a given threshold ϵ_R (resp. ϵ_Q), R-CBFs (resp. R-CBF-QPs) provide set invariance for an inflated version of the safe set, but not necessarily the original safe set. This is demonstrated in Fig. 4b where the only difference from Fig. 4a is that ϵ is increased to 0.2, resulting in the R-CBF and R-CBF-QP state trajectories (purple and orange) leaving the safe set. Similarly, if the estimation error is above a threshold ϵ_M , no MR-CBF will exist, as shown by the MR-CBF state trajectory



(a) GUARDIAN is less conservative than MR-CBFs and R-CBFs, and safer than R-CBF-QPs.



(b) GUARDIAN effectively handles larger state estimate errors (i.e., from adversarial attacks) than MR-CBFs, R-CBFs, and R-CBF-QPs.

Fig. 4: GUARDIAN outperforms MR-CBFs, R-CBFs, and R-CBF-QPs in defense against adversarial attacks.

(pink) in Fig. 4b resulting from failed optimizations. In contrast, GUARDIAN effectively handles the increase in ϵ , with performance similar to that in Fig. 4a, but with more conservativeness to account for the increase in state uncertainty. Details on the specification of ϵ_M , ϵ_R , and ϵ_Q can be found in [17], [18], and [19], respectively, but the existence of these bounds limits the applicability of these approaches in the presence of adversarial attacks. In such settings, the estimation error is typically larger than that present due to random noise or estimation error attributed to imperfect learning, so safety violations are more likely.

V. CONCLUSION

This paper presented GUARDIAN: a reachability-based safety filter that incorporates state uncertainty resulting from noisy measurements to defend ONFLs from adversarial attacks. Specifically, GUARDIAN uses advanced NNV tools to determine a set containing all possible true states given a known attack strength and finds a maximally safe control over the entire safe set. We demonstrated various properties of GUARDIAN with three sets of results, including a realistic runway taxiing problem with image observations, and a problem comparing our approach with existing measurement-robust approaches. In future work, we will seek to improve the scalability of our approach by considering multidimensional inputs and incorporating modern reachability approaches that leverage learned and latent representations.

REFERENCES

- [1] Singh, B., Kumar, R., and Singh, V. P., “Reinforcement learning in robotic applications: a comprehensive survey,” *Artificial Intelligence Review*, Vol. 55, No. 2, 2022, pp. 945–990.
- [2] Szegedy, C., Zaremba, W., Sutskever, I., Bruna, J., Erhan, D., Goodfellow, I., and Fergus, R., “Intriguing properties of neural networks,” 2014, arXiv:1312.6199 [cs].
- [3] Bak, S., Bogomolov, S., Hekal, A., Krish, V., Mata, A., and Rahmati, A., “Zero-One Attack: Degrading Closed-Loop Neural Network Control Systems using State-Time Perturbations,” 2024 ACM/IEEE 15th Int. Conf. on Cyber-Physical Sys. (ICCPs), IEEE, 2024, pp. 12–22.
- [4] Robey, A., Ravichandran, Z., Kumar, V., Hassani, H., and Pappas, G. J., “Jailbreaking LLM-Controlled Robots,” 2025 IEEE Int. Conf. on Robotics and Automation (ICRA), 2025, pp. 11948–11956.
- [5] Zhang, H., Weng, T.-W., Chen, P.-Y., Hsieh, C.-J., and Daniel, L., “Efficient Neural Network Robustness Certification with General Activation Functions,” *Advances in Neural Inf. Processing Systems*, Vol. 31, 2018.
- [6] Xu, K., Shi, Z., Zhang, H., Wang, Y., Chang, K.-W., Huang, M., Kailkhura, B., Lin, X., and Hsieh, C.-J., “Automatic Perturbation Analysis for Scalable Certified Robustness and Beyond,” *Advances in Neural Inf. Processing Systems*, Vol. 33, 2020, pp. 1129–1141.
- [7] Deepmind, “jax_verify: Neural network verification in jax,” 2020.
- [8] Rober, N. and How, J. P., “Constraint-Aware Refinement for Safety Verification of Neural Feedback Loops,” *IEEE Control Systems Letters*, Vol. 8, 2024, pp. 3219–3224.
- [9] Wang, X., Chen, L., Liu, Z., Li, M., and Yin, B., “Verifying Neural Network Controlled Systems by Combining Forward and Backward Reachability Analysis,” 2025 25th Int. Conf. on Software Quality, Reliability and Security (QRS), 2025, pp. 315–326, ISSN: 2693-9177.
- [10] Katz, S. M., Corso, A. L., Strong, C. A., and Kochenderfer, M. J., “Verification of Image-Based Neural Network Controllers Using Generative Models,” *Journal of Aero. Inf. Sys.*, Vol. 19, No. 9, 2022, pp. 574–584.
- [11] Lin, A., Pinto, A., and Bansal, S., “Robust Verification of Controllers under State Uncertainty via Hamilton-Jacobi Reachability Analysis,” 2025, arXiv:2511.14755 [cs].
- [12] Hsu, K.-C., Hu, H., and Fisac, J. F., “The Safety Filter: A Unified View of Safety-Critical Control in Autonomous Systems,” *Annual Review of Control, Robotics, and Auto. Sys.*, Vol. 7, No. 1, 2024, pp. 47–72.
- [13] Wabersich, K. P., Taylor, A. J., Choi, J. J., Sreenath, K., Tomlin, C. J., Ames, A. D., and Zeilinger, M. N., “Data-Driven Safety Filters: Hamilton-Jacobi Reachability, Control Barrier Functions, and Predictive Methods for Uncertain Systems,” *IEEE Control Sys. Magazine*, Vol. 43, No. 5, 2023, pp. 137–177.
- [14] Mahesh, K., Paine, T. M., Greene, M. L., Rober, N., Lee, S., Monteiro, S. T., Annaswamy, A., Benjamin, M. R., and How, J. P., “Safe Autonomy for Uncrewed Surface Vehicles Using Adaptive Control and Reachability Analysis,” *IEEE Trans. on Control Sys. Technology*, Vol. 33, No. 6, 2025, pp. 2334–2349.
- [15] Ames, A. D., Xu, X., Grizzle, J. W., and Tabuada, P., “Control barrier function based quadratic programs for safety critical systems,” *IEEE Trans. on Automatic Control*, Vol. 62, No. 8, 2016, pp. 3861–3876.
- [16] Bansal, S., Chen, M., Herbert, S., and Tomlin, C. J., “Hamilton-Jacobi reachability: A brief overview and recent advances,” 2017 IEEE 56th Annual Conf. on Decision and Control (CDC), 2017, pp. 2242–2253.
- [17] Dean, S., Taylor, A., Cosner, R., Recht, B., and Ames, A., “Guaranteeing Safety of Learned Perception Modules via Measurement-Robust Control Barrier Functions,” *Proceedings of the 2020 Conf. on Robot Learning*, PMLR, 2021, pp. 654–670, ISSN: 2640-3498.
- [18] Nanayakkara, R., Ames, A. D., and Tabuada, P., “Safety Under State Uncertainty: Robustifying Control Barrier Functions,” 2025, arXiv:2508.17226 [eess].
- [19] Das, E., Nanayakkara, R., Tan, X., Bena, R. M., Burdick, J. W., Tabuada, P., and Ames, A. D., “Safe Navigation under State Uncertainty: Online Adaptation for Robust Control Barrier Functions,” 2025, arXiv:2508.19159 [eess].
- [20] Lin, R. and Egerstedt, M., “Stochastic Control Barrier Functions under State Estimation: From Euclidean Space to Lie Groups,” *arXiv preprint arXiv:2601.16198*, 2026.
- [21] Isaacs, R., “Differential games i: Introduction,” Tech. rep., 1954.
- [22] Bansal, S. and Tomlin, C. J., “DeepReach: A Deep Learning Approach to High-Dimensional Reachability,” 2021 IEEE Int. Conf. on Robotics and Automation (ICRA), 2021, pp. 1817–1824, ISSN: 2577-087X.
- [23] Nakamura, K., Peters, L., and Bajcsy, A., “Generalizing Safety Beyond Collision-Avoidance via Latent-Space Reachability Analysis,” 2025, arXiv:2502.00935 [cs].
- [24] Schmerling, E., “hj reachability: Hamilton-jacobi reachability analysis in jax,” 2024.

[25] Cintrón-Arias, A., Banks, H. T., Capaldi, A., and Lloyd, A. L., “A Sensitivity Matrix Based Methodology for Inverse Problem Formulation,” 2020, arXiv:2004.06831 [stat].